

Performance optimisation for drift-robust fidelity improvement of two-qubit gates

G. A. L. White[†], C. D. Hill[†], and L. C. L. Hollenberg^{†*}

[†]*School of Physics, University of Melbourne, Parkville, VIC 3010, Australia*

Quantum system characterisation techniques represent the front-line in the identification and mitigation of noise in quantum computing, but can be expensive in terms of quantum resources and time to repeatedly employ. Another challenging aspect is that parameters governing the performance of various operations tend to drift over time, and monitoring these is hence a difficult task. One of the most promising characterisation techniques, gate set tomography (GST), provides a self-consistent estimate of the completely positive, trace-preserving (CPTP) maps for a complete set of gates, as well as preparation and measurement operators. We develop a method for performance optimisation seeded by tomography (POST), which couples the power of GST with a classical optimisation routine to achieve a consistent gate improvement in just a short number of steps within a given calibration cycle. By construction, the POST procedure finds the best available gate operation given the hardware, and is therefore robust to the effects of drift. Further, in comparison to other quantum error mitigation techniques, it builds upon a one-time application of GST. To demonstrate the performance of this method on a real quantum computer, we map out the operations of six qubit pairs on the superconducting *IBM Q Poughkeepsie* quantum device. Under the restriction of logical-only control, we monitor the performance of the POST approach on a chosen CNOT gate over a period of six weeks. In this time, we achieve a consistent improvement in gate fidelity, averaging a fidelity increase of 21.1% as measured by randomised benchmarking. The POST approach should find wide applicability as it is hardware agnostic, and can be applied at the upper logical level or at a deeper pulse control level.

INTRODUCTION

The nascent field of quantum computing has seen an emergence of many experimentally realised small-scale devices in recent years, most notably in superconducting qubit systems and trapped atomic spins [1–5]. Different architectures have achieved high fidelity one and two-qubit gates, as well as the construction of multi-qubit entangled states [2, 6–12]. Despite this progress, current hardware cannot yet demonstrate large-scale topological quantum error correction below threshold, and there are many significant obstacles to overcome before qubit numbers can be scaled up to useful levels. Quantum computers presently face the challenge of imperfections in state-preparation, measurement errors, and erroneous logical gates. Before improvement can be achieved, comprehensive characterisation techniques are essential in mapping where deficiencies lie.

Noise on real quantum devices is challenging to understand quantitatively. In particular, it is difficult to isolate device behaviour given the tendency of noise and system parameters to *drift* [13–15]. This is one of the many barriers facing the improvement of quantum hardware. Common characterisation techniques such as quantum process tomography (QPT) [16] and randomised benchmarking (RB) [17] offer an insight into the quality of a qubit, but suffer from respective self-consistency and limited-information issues. Gate set tomography (GST), introduced in [18, 19], provides a relatively novel method in which the preparation, gate, and measurement operations can be implemented in conjunction with each other and separately characterised. The results can be highly accurate, but with the trade-off that a large number of

experiments are required to provide the data. The analysis itself is also computationally resource-demanding. As a consequence, there are relatively few examples of two-qubit GST carried out experimentally in the literature [20–22].

Two-qubit gates are the most significant source of error in many quantum circuits, and so minimising their infidelity is critical to the performance of quantum algorithms. In this manuscript, we develop a method for performance optimisation seeded by tomography (POST) to consistently improve two-qubit CNOT gates based on a hybrid quantum-classical approach. We characterise the bare two-qubit logic gate using GST, find the optimal corrective parameters within a given noise parametrisation model based on bookend single-qubit unitaries, and then use these as a seed to the Nelder-Mead algorithm in order to find the best improvement for a given calibration cycle. Following the one-time overhead of GST, each daily optimisation is performed in a small (<150) number of experiments to overcome any drift which has occurred. We test the method on the *IBM Q Poughkeepsie* quantum device. The coupling of the GST seed with classical optimisation is successful at improving the gate. When tested on an experimental device, we find the POST approach is effective even weeks after the initial characterisation. The hybrid technique brings the gate as close as possible to its target, up to the hardware limit, but the actual effectiveness depends on the level of control afforded. Although GST has previously been proposed as part of a quantum error mitigation protocol in [21] and [23], we emphasise the need to avoid repeated application of GST in any gate-improvement techniques, owing to its extremely high experimental and computa-

tional overheads.

We performed our experiments on an IBM cloud-based quantum computer with only logical-level control. As a consequence, corrections to the CNOT could only be made through single qubit gate corrections, which themselves were erroneous. With control of the CNOT pulse scheme, the corrections could be more effective.

In addition to the testing of the POST gate improvement scheme on a specific two-qubit case, we also conducted two-qubit GST experiments on six separate CNOT gates as an investigation into the performance and types of noise to occur on real superconducting devices. Understanding the real noise that occurs on devices is important for several reasons: It can help inform future characterisation, which results in these procedures being less computationally expensive; it can help understand noise channels, which is important for quantum error correction [24]; and it can help identify hardware issues up on a real machine for better future implementation [1]. We present these results, as well as a theoretical evaluation of the effectiveness of our technique on the additional qubit pairs.

AN OVERVIEW OF GATE SET TOMOGRAPHY

Gate set tomography is a hardware-agnostic method of characterising quantum operations. This section provides a brief overview of its methodology – for a comprehensive guide to the techniques involved, see [1, 25]. In this work, we operate in the Pauli transfer matrix (PTM) representation of quantum channels. The matrices in this representation are mappings of the Stokes vector of a given density matrix. For some map Λ , whose action on a density matrix ρ has a Kraus decomposition $\Lambda(\rho) = \sum_i K_i \rho K_i^\dagger$, this matrix representation is given by:

$$(R_\Lambda)_{ij} = \text{Tr}(P_i \Lambda(P_j)), \quad (1)$$

where the $P_{i,j}$ refer to the normalised, ordered set of Pauli matrices spanning the d^2 -dimensional space of bounded linear operators on some Hilbert space \mathcal{H}_d . That is, the n -qubit basis is the set

$$\mathcal{P}_n = \{I/\sqrt{2}, X/\sqrt{2}, Y/\sqrt{2}, Z/\sqrt{2}\}^{\otimes n} \quad (2)$$

The maps can be visualised as isolating eigenvectors of the P_j as the input, and taking the P_i expectation value of the output. Applying the superoperator formalism makes this picture more convenient. Here, density matrices are represented as d^2 -dimensional vectors $|\rho\rangle\rangle$ on a Hilbert-Schmidt space with inner product $\langle\langle \rho_1 | \rho_2 \rangle\rangle = \text{Tr}(\rho_1^\dagger \rho_2)$. This allows the action of quantum channels to be given by ordinary matrix multiplication. The k th component of these vectors is equal to $\text{Tr}(P_k \rho)$.

The operational action is given by $|\Lambda(\rho)\rangle\rangle = R_\Lambda |\rho\rangle\rangle$ and map composition by $R_{\Lambda_2 \circ \Lambda_1} = R_{\Lambda_2} \cdot R_{\Lambda_1}$.

The only experimentally accessible quantities in a laboratory are measurements of a quantum state. For example, after a sequence of quantum operations G , many measurements are taken in order to form an estimate of

$$\langle\langle E | G | \rho \rangle\rangle \quad (3)$$

for some preparation Hilbert-Schmidt vector $|\rho\rangle\rangle$ and some measurement effect $\langle\langle E |$. Quantum process tomography is a technique which provides an estimate for G by acting the operator on a complete set of preparations, followed by a complete set of basis measurements. This style of characterisation assumes perfect state preparation and measurement (SPAM). When SPAM errors are not negligible, however, QPT produces gate estimates considerably far away from the true maps [25]. This is particularly an issue since the primary source of error in current quantum computers are SPAM errors. RB curves administer a metric for the quality of a gate operation, but provide no information as to how that gate might be improved. Furthermore, since it is insensitive to SPAM errors, there is little or no information produced about the character of SPAM on a device. The ideal characterisation should produce an accurate picture of all quantum channels, including projection operations.

GST aims to fully characterise a complete set of gates. The self-consistency in this method is achieved by including the preparation and measurement operations within the gateset $\{|\rho\rangle\rangle, \langle\langle E |, G_0, G_1, \dots\}$. A set of gates is chosen firstly as the object of characterisation. The only requirement is that these operations (or their compositions) generate an informationally complete set of preparations and measurements. That is, they form a complete basis of the Hilbert-Schmidt space. These SPAM operations are known as *fiducials*, and are denoted by $\mathcal{F} = \{F_0, F_1, \dots, F_n\}$. They are optimally selected to form the most mutually distinguishable informationally complete set. Further, a set of gate compositions $\mathcal{G} = \{g_0, g_1, \dots, g_n\}$ is generated. The elements of this set are termed *germs*, and each comprises a sequence of operations from the gateset. Gates contain a large number of free-parameters, and the emergence of errors in these depend on the input state, sequence of operations, and basis in which a measurement is made. Germs are chosen from an extensive search such that a possible error in each gate parameter may be amplified and made detectable by the repetition of at least one germ. In order to reduce the statistical error in detecting noise, each germ is repeated L times for many different values of L . When every possible noisy parameter is made detectable, the germs set is termed *amplificationally complete* [1]. For all values of i, j, k , and L , the experimental data are then collected in the object

$$p_{ij}^L = \langle\langle E | F_i^{(\text{prep})} g_j^L F_k^{(\text{meas})} | \rho \rangle\rangle. \quad (4)$$

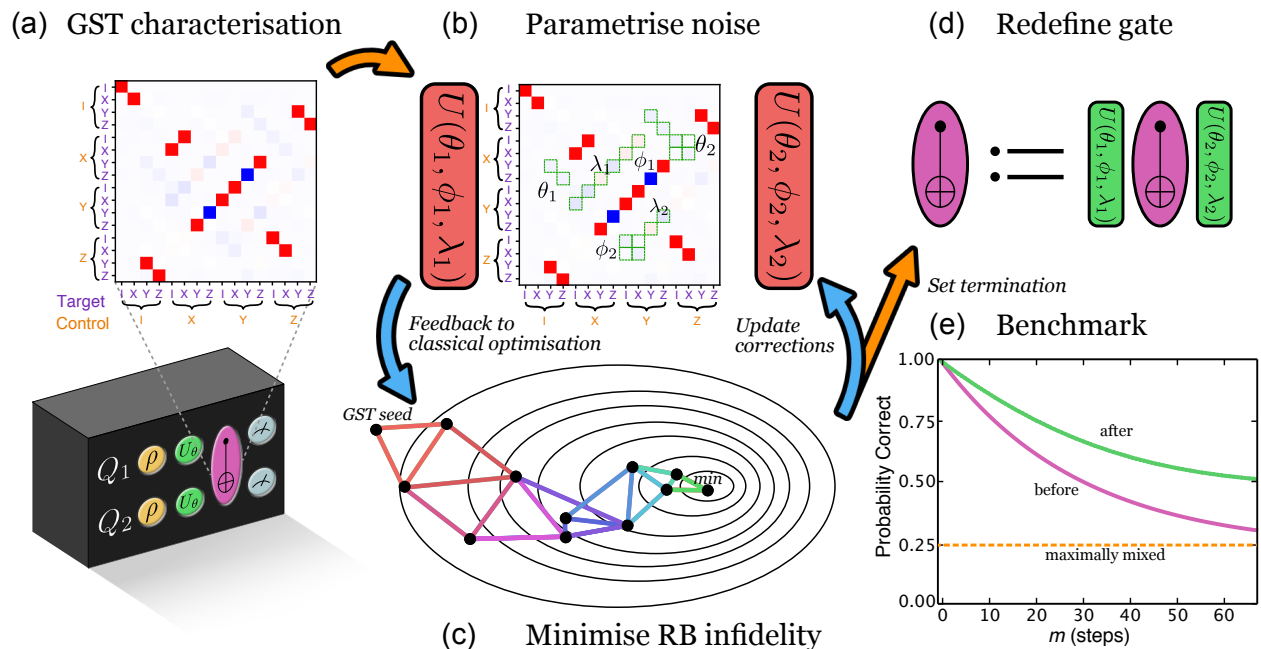


FIG. 1: Overview of the POST approach for CNOT gate fidelity improvement. (a) Initial characterisation of the CNOT Pauli transfer matrix (PTM) using gate set tomography. (b) Gate noise is parametrised in the action of arbitrary single-qubit unitaries acting before and after the CNOT gate. The parameters that minimise the Frobenius distance between the noisy and ideal CNOT gates are then found. (c) These parameters then seed a Nelder-Mead optimisation, where the objective function is the experimental infidelity of a chosen length randomised benchmarking experiment. With each iteration of POST, a new simplex is chosen and the randomised benchmarking experiment is performed for each vertex with the single qubit unitaries taking on the parameters at that point. (d) When the minimum infidelity is found, the CNOT gate is redefined to include the corrective unitaries. (e) The new gate is then fully benchmarked against the native gate, showing a revived fidelity for a much larger number of applications.

Linear inversion can provide an estimate of each gate at this point, but there is no natural way to include physicality constraints or to select the correct gauge. A maximum likelihood estimate (MLE) is therefore performed to provide the best estimate for the experimental gate-set, consistent with (4), which obeys the conditions of complete positivity and trace preservation.

GST provides a device-independent estimate of the quantum channel. Like all characterisation processes, it assumes a model of the physical process taking place. The model assumption is purely Markovian, including zero leakage and weak environmental couplings – that maps are composable and without context dependence. When violations of these model assumptions show up in the data, the non-Markovianity is then flagged and the data artificially deprecated. It is for this reason that the GST estimates must be treated with care: in physical terms, a quantum operation cannot necessarily be treated in isolation and a circuit decomposed into its constituent maps.

IMPROVEMENT OF GATE-SET PARAMETERS

The CPTP map of quantum gates given by GST highlight all Markovian errors in the operation. Examples of errors of this nature include control errors, such as axis tilt or errors in pulse shaping, or erroneous coherent rotation of the qubits due to external couplings.

The best method in which to address these noisy parameters depends on the level of control afforded in the device. Given the recent advent of cloud-based NISQ computers, where users only have restricted control of the device, the POST protocol introduced here makes use only of additional logical operations on the qubits (although we note in the conclusion that the extension to high-level pulse control is possible). At the time of the experiments, this was the only control available to the authors, and so the only scheme examined. With pulse level control, provided by IBM through OpenPulse, however, the proposed blueprint could be straightforwardly modified to absorb the corrections into the definition of the gate – rather than applying logical corrections around it. We summarise the overall POST procedure in Figure 1, and describe it in further detail here.

GST provides a means by which errors can be identified, but it is not necessarily straightforward to then mitigate their effects. Errors occurring on two-qubit gates such as a CNOT tend to be an order of magnitude greater than those of single qubits. From the perspective of logical corrections, it is therefore optimal to address two-qubit noise with the application of single-qubit gates.

Consider a quantum device with an informationally complete set of two-qubit controls. This can be used to conduct a GST experiment in the standard way on a qubit pair. The GST analysis of a CNOT produces an estimate for the CPTP map of the experiment, designated by \bar{G}_{CX} . This can be decomposed into the product of an ideal CNOT, G_{CX} , and some residual noise channel G_Λ – the inverse of which is generally unphysical [26]. Previous approaches have typically treated this noise with quasiprobability decompositions [27]. In the case of solely logical control, the nearest physical corrective G_Λ^{-1} map may not be within the user’s control-set. Importantly, given gate calibration and general hardware drift, a GST estimate’s accuracy quickly expires over time. Solely utilising GST will require a significant overhead every time the corrections are implemented. From this, it is clear that GST on its own faces limitations as a practical method of improving gates.

Without direct control of the hardware, correcting all two-qubit errors will not be possible, since these corrections will contain associated errors equal or greater in magnitude than the existing ones. In this control regime we propose placing single qubit corrective gates before and after the native CNOT in order to correct as much of the local noise as possible, and then optimising over their parameters. Using a unitary parametrisation for the four correction gates U_i ($i \in \{1, 2, 3, 4\}$)

$$U_i(\theta_i, \phi_i, \lambda_i) = \begin{pmatrix} \cos(\theta_i/2) & -e^{i\lambda_i} \sin(\theta_i/2) \\ e^{i\phi_i} \sin(\theta_i/2) & e^{i\lambda_i+i\phi_i} \cos(\theta_i/2) \end{pmatrix}, \quad (5)$$

We propose a super-logical CNOT gate structured as

$$(U_1 \otimes U_2) \cdot \bar{G}_{CX} \cdot (U_3 \otimes U_4), \quad (6)$$

provided that the cumulative error of four single qubit gates is not greater than one two qubit gates. In the case of high single qubit error rates (or cross-talk between simultaneous gates), a similar approach can be made by applying local corrections exclusively on the control qubit, at the expense of more limited noise-targeting. That is,

$$(U_1 \otimes \mathbb{I}) \cdot \bar{G}_{CX} \cdot (U_2 \otimes \mathbb{I}). \quad (7)$$

In order to clearly see the difference between corrections on both qubits versus corrections acting solely on the control qubit, we illustrate the addressable parts of the CNOT matrix in green in Figures 2c and 2d.

The ϕ_i , θ_i , λ_i are first selected with a simple optimisation to minimise the Frobenius distance between the corrected gate and the ideal map,

$$\|U_1 \otimes U_2 \cdot \bar{G}_{CX} \cdot U_3 \otimes U_4 - G_{CX}\|_F. \quad (8)$$

If the GST estimates of a quantum process were perfect and static with time, then this would be sufficient to have an improved CNOT gate. However, because GST is only an estimate of a Markovian map within a (generally) non-Markovian system, a simple mathematical minimisation will not necessarily result in a physical optimisation.

Instead, what we propose is a tune-up procedure which optimises the *performance* of the gate by using GST to identify the most critical parameters. As such, it is robust to the drift of different noisy parameters and does not rely on the absolute accuracy of the GST estimate. The only assumption is that the noisy parameters will remain structurally similar enough to those of the GST estimate, that an optimisation seeded by GST will bring us back to a better gate than the native operation in few iterations. We define our objective function as the RB infidelity of the gate, in order to make use of the most general metric of performance.

The algorithm to implement the POST procedure is as follows:

1. Conduct a series of experiments given by the requirements of GST. Use these to produce an output estimate of the gate’s PTM.
2. Using a classical minimisation technique, find the six or twelve parameters which numerically minimise the Frobenius distance between the super-logical and the ideal CNOT gates, given in Expression (8). These will be the seed parameters. The choice of the Frobenius distance is not necessarily special, but we elected to use it to make the resulting matrices as similar as possible.
3. Define the objective function to be a probability of success of some length m RB experiment. Taking Step 2. as a newly defined CNOT gate, compute the objective function for both the native and new CNOT gates as a point of comparison. Using the parameters obtained from GST as a seed, perform an optimisation of the CNOT gate by feeding the parameters into the Nelder-Mead algorithm, where for each vertex of the simplex, the m -length RB infidelity is computed as the objective function.
4. Converge at some pre-defined level of change. The newly improved CNOT gate is then defined by the composition of the final single qubit unitary gates on either side of the native CNOT gate.
5. Conduct a full RB experiment to compare the new gate fidelity to the original.

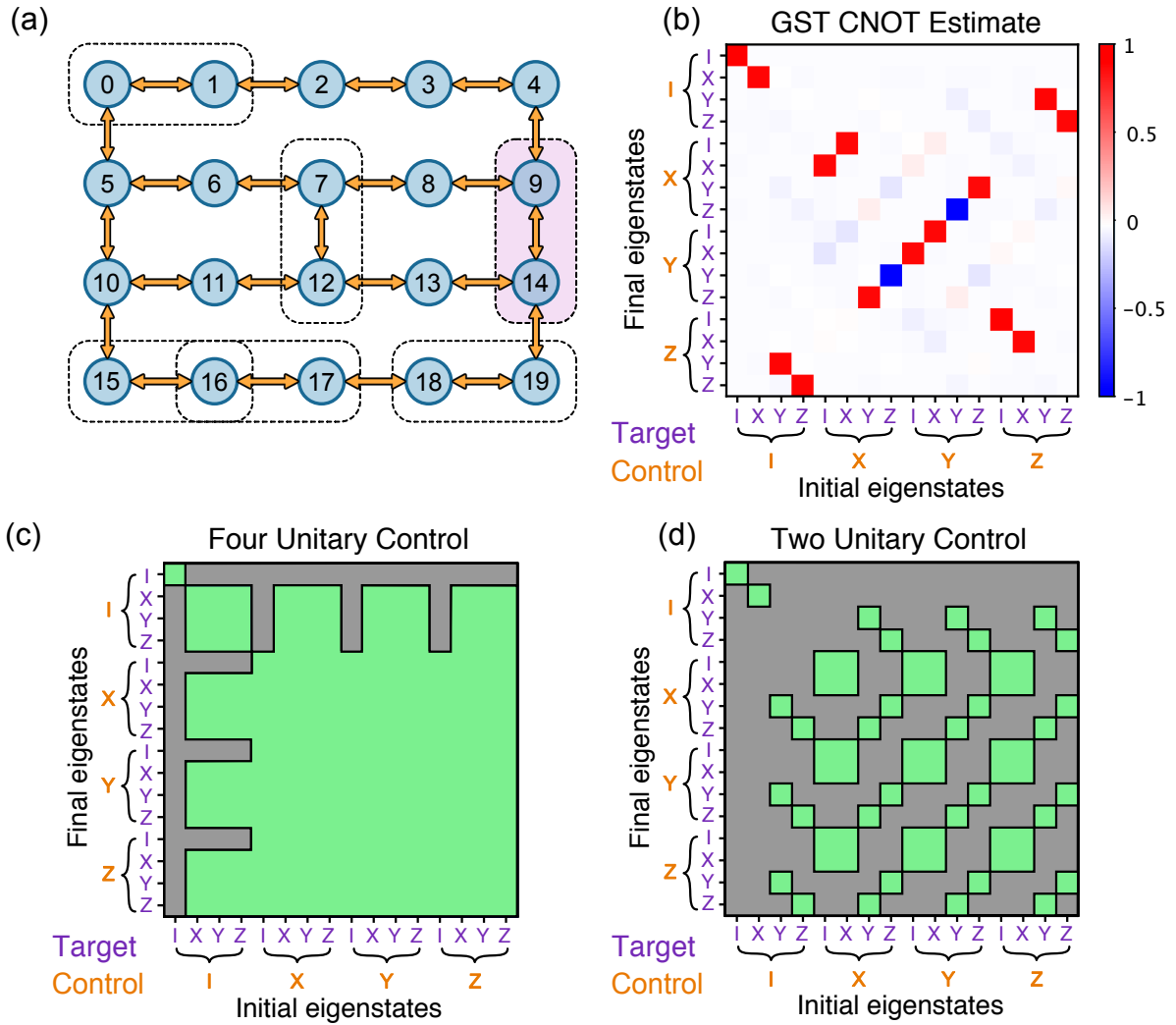


FIG. 2: (a) The *IBM Q Poughkeepsie* device layout, showing both the geometry and connectivity. Dotted lines indicate the six pairs of qubits that were characterised under GST. Qubits 9 and 14 (highlighted in pink) were chosen as the subject for testing POST. (b) The GST reconstructed estimate of the PTM of the 14-9 CNOT gate under investigation. (c) The green parts of this matrix indicate the controllable parts of the overall map when combining single-qubit operations on the control and target qubits both before and after the native CNOT. Under this regime, almost all coherent noise is addressable in principle. (d) The green parts of this matrix indicate the controllable parts of the map when restricted to single-qubit operations on the control qubit before and after the native CNOT. This regime is far more restrictive than the previous for the trade-off of introducing approximately half of the amount of single-qubit error.

The overview of the procedure is to use the GST estimate as a seed for the Nelder-Mead optimisation algorithm, which then works to minimise the infidelity of the CNOT gate by varying the parameters given in (6) or (7). We take the infidelity measure to be a set of fixed m -length randomised benchmarking experiments. In a short number of iterations, this locates the optimal corrective rotations to make for a given day. This process is summarised in Figure 1. The flexibility of the procedure is not only its robustness to drift, but generic steps (optimisation procedure, noise parametrisation, objective function) can all be chosen at the user's discretion.

EXPERIMENTAL IMPLEMENTATION

We tested the POST framework for CNOT characterisation and improvement on the 20 qubit *IBM Q Poughkeepsie* superconducting quantum device. Two qubit GST was performed on six pairs of qubits with the gate-set $\{\mathbb{I}, G_{XI}(\frac{\pi}{2}), G_{IX}(\frac{\pi}{2}), G_{YI}(\frac{\pi}{2}), G_{IY}(\frac{\pi}{2}), G_{CX}\}$ up to a germ repetition of $L = 8$ for a total of 20,530 circuits at 8190 shots each. The layout and connectivity of this device is shown in Figure 2a. We also indicate the qubits on which experiments were performed. Us-

ing the notation ‘control-target’ to indicate the physical qubit pair used respectively as the control and target of a CNOT gate, we characterised the gates of qubits 0-1, 12-7, 14-9, 15-16, 16-17, and 18-19. We then elected to test the POST procedure on the gate which had most recently been characterised, for which the control was qubit #14 and target qubit #9. For the germ generation and MLE steps, we used the comprehensive open source Python package *pyGSTi*, introduced in [28]. With the tools available, we generated the required germs from our target gatesets, and conducted the analysis of our experimental data. The GST estimate from the 14-9 qubits, used hereon in the POST tests, is shown in Figure 2b. The resulting noise maps for each additional CNOT gate can be found later in this manuscript, in Figure 4.

Results Summary – The initial GST analysis of the 14-9 CNOT gate took place on the 31st of March, 2019 and its corrective parameters used as the base vertex for the Nelder-Mead simplex method. The procedure was implemented a total of 12 times over a period of approximately six weeks, corresponding to overlap with approximately 40 different calibration cycles. Figure 3a displays a summary of the improvement shown over the native gate with each experiment run, which we define as $r_u/r_c - 1$ for bare RB infidelity r_u and corrected RB infidelity r_c . In each case, both the corrected and uncorrected benchmarking experiments were conducted in the same job submission to avoid any bias in gate drift throughout the day. The total average improvement was 21.1%, with a notable outlier of 61.8% in experiment 10. The median observed improvement was 19.1%. In the next section we discuss how this compares to theoretical figures based on the GST estimates. Figure 3b is a comparison RB curve showing the decay of an example improved gate over the native fidelity. For clarity and comparison, we also plot example curves with 10% and 0.1% error rates. Note that this RB number is from the overall curve, which is composed of single and two-qubit gates. For these experiments, this partitions into $r = 3/4 \cdot r_{\text{CNOT}} + 1/4 \cdot r_{\text{single}}$. To reduce the total number of experiments per day, we did not compute multiple curves with different fractions of CNOT and single qubit gates. Consequently, $r_u/r_c - 1$ is really $(3/4 \cdot r_{u,\text{CNOT}} + 1/4 \cdot r_{\text{single}}) / (3/4 \cdot r_{c,\text{CNOT}} + 1/4 \cdot r_{\text{single}}) - 1$, which is a lower bound for the improvement of the CNOT gate. Given that $r_{\text{single}} < r_{\text{CNOT}}$ by about an order of magnitude, we do not expect that the figure differs substantially.

The minimised objective function was the average infidelity of 20 randomly sampled RB circuits, consisting of 16 circuit layers in addition to the preparation and measurement layers. Each circuit was run at 8190 shots in order to minimise statistical error in the optimisation. The use of an RB experiment as the objective function is a flexible metric and can be chosen as the user desires. In principle, context-dependence of a gate may affect the

versatility of the improved gate, however at this stage RB curves are the most robust assessment of a gate’s performance and require the fewest assumptions.

In the Nelder-Mead method, a dimension 6 simplex with 7 vertices is constructed, with the base vertex given by the GST parameters. The objective function is then evaluated for each point. In our case, we formed a simplex with each vertex designated a distance of 0.1 in each orthogonal direction. What follows are four possible steps known as reflection, expansion, contraction, and shrinking. The scale of each is given respectively by the adaptive parameters $\alpha = 1$, $\beta = 1 + 2/d$, $\gamma = 0.75 - 1/2d$, and $\delta = 1 - 1/d$ chosen from [29], where d is the dimension of the search.

The evaluation of the first three are each contingent on what values the objective function takes in previous steps. Rather than submitting a circuit to run at each step before performing the next conditional outcome and then going to the back of the queue, we submitted all possible circuits in the single iteration – in this case, 11 circuits – and then performed the classical steps with the data afterwards. In order to save on computation, we elected to omit the shrink step. After five iterations of no further improvement we would then terminate the algorithm and redefine our gate with the best point.

We used a relatively new form of RB known as *direct randomised benchmarking* (DRB) [30]. In a single circuit, DRB prepares stabiliser states, followed by m randomly selected layers of gates native to that stabiliser, before finally performing a stabiliser measurement to give the success probability. A number of randomly generated circuits can then be used to provide an overall average. The utility of this over Clifford RB is the ability to specify the occurrence of given gates. Here, we randomly generated 20 RB circuits, with CNOT gates composing on average 3/4 of the total circuit. The average probability of success at length m , P_m is then plotted over a series of values for m . These points are then fit to $P_m = A + Bp^m$ for fit parameters A, B , and p . The RB number $r = (15/16)(1 - p)$ is then the probability of an error occurring under a stochastic model.

Tracking Drift – Operating on the assumption that this method finds the most appropriate corrective parameters on a particular day, we can use this data to loosely quantify the amount of drift on a real quantum information processor (QIP), and *a posteriori* examine our assumptions. The most direct witness for drift in our results is in the slight change of the corrective parameters day-to-day, the quantities of which are provided in Table I. Inspection of these values, however, is not necessarily illuminating. Moreover, the variables do not all independently affect the final map, meaning that change in the parameters themselves might obfuscate the fact that the channel overall has not varied much.

In order to paint a more concrete picture of the effects of the parameters, we study the case of the improved

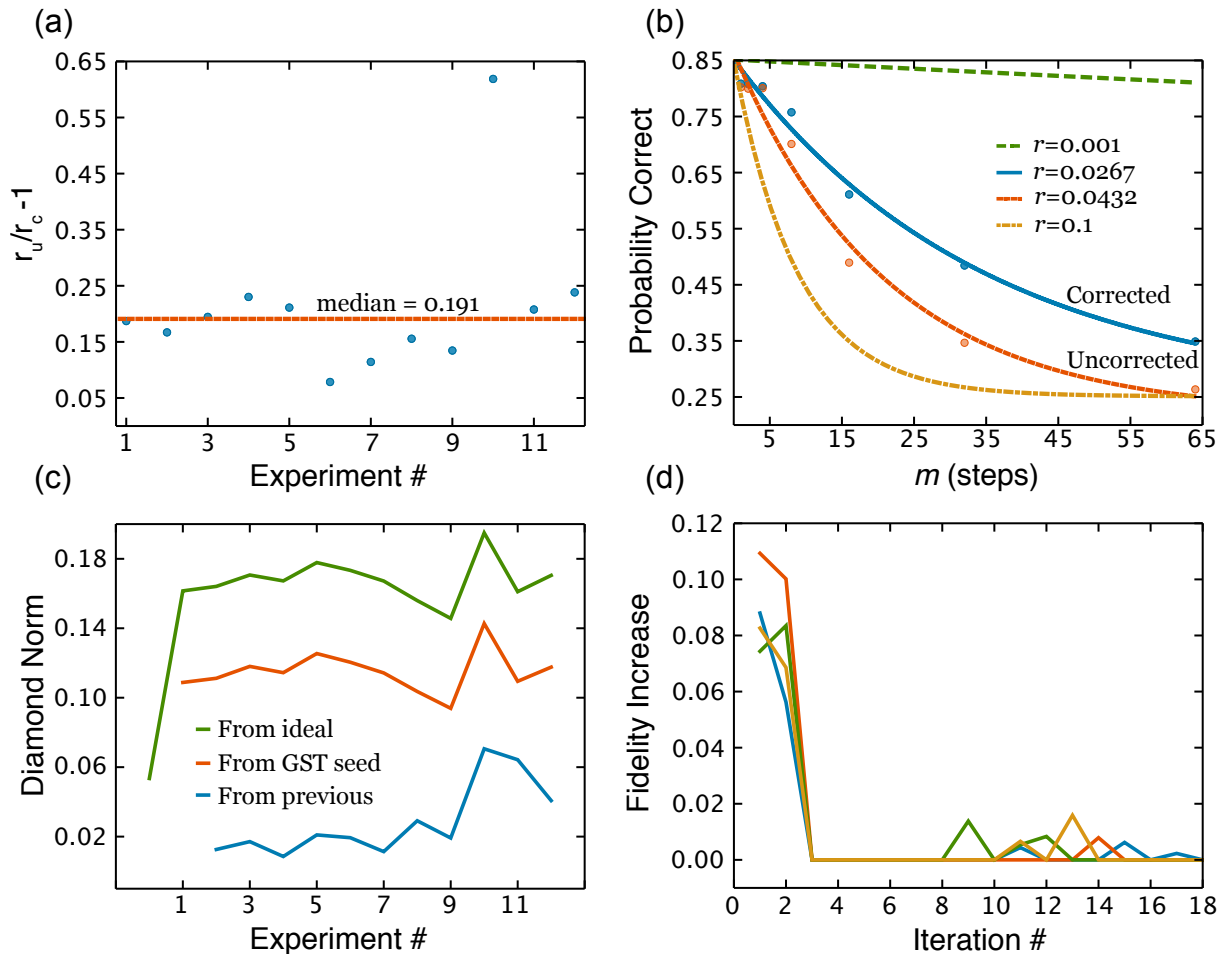


FIG. 3: Efficacy and robustness of the POST protocol – experimental test on the 14-9 CNOT gate. (a) Improvement values for each experiment taken over the six week period. The orange dotted line also indicates the median improvement value. (b) Example RB curve showing our best improved CNOT gate decay vs. the native gate RB experiment for experiment 10 (our most emphatic example of gate improvement). Also shown for comparison are theoretical curves corresponding to 10% and 0.1% error rates. (c) A comparison of the diamond norm of the corrective channel over time: firstly with respect to the ideal CNOT, secondly with respect to the initial GST corrections, and finally with respect to each previous experiment. (d) An indication of the convergence speed of the Nelder-Mead gate optimiser for four example runs. This figure shows how the fidelity of the RB experiment increases with each iteration. We observe an initially large increase in the fidelity of the experiment, followed by only small changes thereafter, and zero changes after 18 iterations. The sequence very quickly finds its best gate in a small number of steps.

Date	θ_1	ϕ_1	λ_1	θ_2	ϕ_2	λ_2
31/03/19 (initial GST)	0.046	-1.271	0.480	0.029	0.480	0.393
02/04/19	0.116	-1.234	0.536	0.116	0.545	0.403
09/04/19	0.130	-1.218	0.461	0.084	0.565	0.475
24/04/19	0.116	-1.234	0.552	0.119	0.558	0.415
27/04/19	0.148	-1.208	0.502	0.010	0.530	0.427
29/04/19	0.089	-1.228	0.523	0.071	0.523	0.436
01/05/19	0.218	-1.199	0.552	0.010	0.552	0.365
03/05/19	0.089	-1.228	0.523	0.071	0.523	0.436
10/05/19	0.096	-1.221	0.530	0.079	0.530	0.443
13/05/19	0.141	-1.310	0.497	0.123	0.575	0.488

TABLE I: Values of the corrective parameters obtained after a full improvement cycle for each day of experiments, given to the third decimal place. These correspond to the unitary parametrisation given in Equation (5).

gate as though it comprised three perfect gates. We then compare the diamond distance of this channel from the ideal CNOT, from the initial GST seed, and from the previous experiment. The diamond distance is a means of assessing the distinguishability of two quantum channels. It is a worst-case error rate, taking the largest output trace distance over all possible input matrices. That is, for two quantum channels Φ_1 and Φ_2 :

$$\|\Phi_1 - \Phi_2\|_{\diamond} := \sup_{\rho \in \mathcal{H}^{\otimes 2}} \frac{1}{2} \|\Phi_1(\rho) - \Phi_2(\rho)\|_1, \quad (9)$$

where $\|\cdot\|_1$ is the trace distance, a common measure of distinguishability between two density matrices. This metric between channels is commonly used in fault-tolerance calculations for quantum error-correcting codes. Our results are summarised in Figure 3c. One of the key assumptions in this method was that the system and its gate noise never changed too much from the initial GST seed that the optimiser could not easily find the best gate for the day. The distance of the corrective channel on a given day from the GST seed supports this stance: over a six week period the mean diamond distance is 0.115, with a variance of 1.44×10^{-4} . We also observe between experiments an average change of 0.0273, flagging the presence of drift and motivating the need for such a scheme in the first place.

Convergence Speed – Any error mitigation protocol designed to address drift in a QIP will need to be regularly implemented as part of a tune-up procedure. It is therefore ideal that it require as few experiments as possible. In Figure 3d we present how each iteration of the Nelder-Mead optimisation increased the fidelity of the RB experiment for four sample experiments. In each case, a substantial improvement was found in the first three iterations, beyond which we observed only small fluctuations, and zero change after 18 iterations. Each iteration requires 11 circuits to run, and so most of the improvement was found in 22 circuits, with the worst case requiring approximately 200 – depending on when one accepts the algorithm to terminate. Assuming 1 millisecond per shot, POST would take approximately nine minutes to converge in the worst case scenario. Depending on the cross-talk limitations of the device, it could then be run in parallel across all non-overlapping qubit pairs.

Tomography on other qubit pairs

In addition to gate improvement on qubits 14 and 9 on the *IBM Q Poughkeepsie*, we also performed GST experiments on five other qubit CNOT pairs on the quantum device. This incorporates a further $5 \times 20,530$ circuits at 8190 shots each. We present this data as a case study for the noise that occurs in a real quantum device, and theoretically assess the effectiveness of the POST technique

at mitigating the noise. Here, the fidelities of these gates and their structure indicate whether noise can be addressed by the single-qubit unitaries used. Figure 4 shows the noise PTMs for each of the six CNOT gates investigated. That is, the GST estimate with the ideal CNOT subtracted off to emphasise the noisy parts of the map. The control and target numbers given refer respectively to the qubits of Figure 2a acting as the control and target of the CNOT gate under characterisation. We elected to map out these qubits in order to obtain a relatively uniform sample of the full device geometry. It is instructive to compare these matrix plots with the schematics given in Figures 2c and 2d, which respectively indicate local target/control, and sole control rotations. PTM noise whose locations are correspondingly indicated in green in the schematics can be explained as a local rotation occurring either before or after the CNOT. For example, the block-like features prominent in 0-1 and 15-16 make up the landscape of Figure 2d, suggesting a rotation of Z -eigenstates of the control qubit into X - and Y - eigenstates both before and after the CNOT. Any noise that falls outside the green of either schematic can be attributed either to decoherence or cross-resonance errors.

We also use this data to estimate the effectiveness of the POST procedure on the other qubit-pairs. First, we provide a theoretical maximum fidelity by computing the minimal infidelity of the corrected CNOT, assuming perfect corrective gates. This figure is not realisable on a physical system, and is intended to illustrate how much noise can be simply eliminated in principle. In practice, it is difficult to estimate how errors in the corrective gates will affect the corrections themselves, and so we may only operate under the best case scenario where the infidelity of the single-qubit gates affects the overall fidelity, but sustains perfect corrections. This upper-bound is likely to well exceed the fidelity actually achieved; it operates under the assumption of perfect GST estimates, and that the only lingering errors will be due to the single qubit unitaries as well as the remaining theoretical infidelity of the corrected gate. For example, the estimated maximum improvement for the 14-9 qubit pair was 34.0%, compared to the 21.1% that was actually observed. A summary of the data is provided in Table II. It is interesting to note that the value for this qubit pair is the second lowest of the six, indicating much larger potential upside if we were to repeat the experiment on other sets.

Pulse sequences for the implementation of a CNOT gate typically consist of a local pulse to each qubit, as well as an additional cross-resonance pulse coupling the two. We would expect implementing POST with absorbed corrective rotations into the native CNOT pulse sequence would see a much larger increase in fidelity.

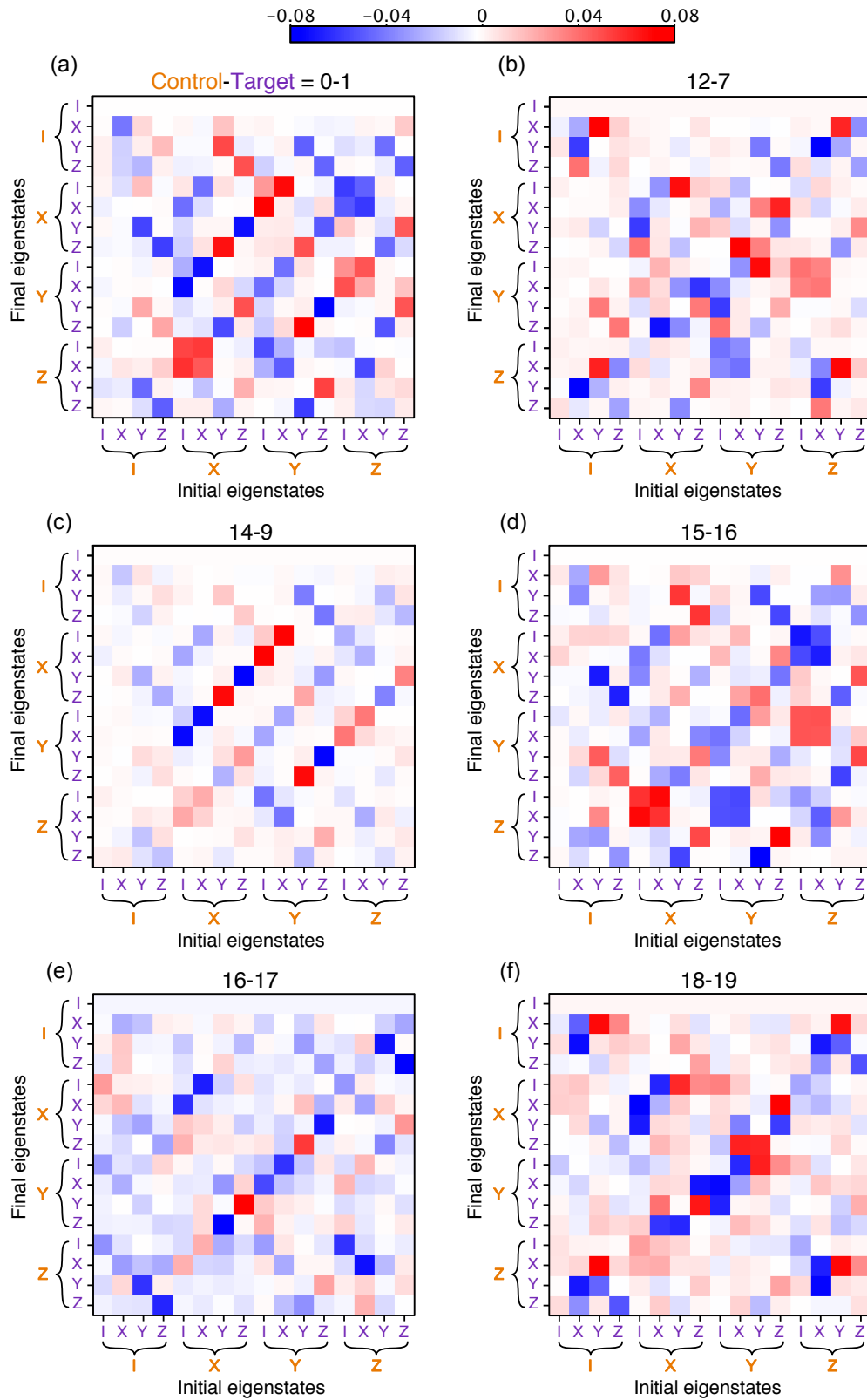


FIG. 4: The matrices here show the GST-estimated PTM representations of the CNOT gate between 6 pairs of different qubits. The control and target designations correspond to the device layout given in Figure 2. In particular, we show the estimate of the actual gate with the ideal CNOT subtracted off in order to emphasise the extraneous values occurring in the map.

Qubit pair (control-target)	r_{single}	r_{CNOT}	Theoretical minimum r_{CNOT}	Estimated minimum r_{CNOT}	Estimated maximum improvement (%)
0-1	5.36×10^{-3}	1.58×10^{-2}	6.52×10^{-4}	1.13×10^{-2}	38.9
12-7	9.37×10^{-3}	2.35×10^{-2}	7.18×10^{-4}	1.94×10^{-2}	21.1
14-9	6.19×10^{-3}	1.91×10^{-2}	1.97×10^{-3}	1.43×10^{-2}	34.0
15-16	5.66×10^{-3}	2.08×10^{-2}	1.65×10^{-3}	1.29×10^{-2}	60.9
16-17	8.35×10^{-3}	4.55×10^{-2}	3.44×10^{-4}	1.70×10^{-2}	167.9
18-19	4.55×10^{-3}	1.76×10^{-2}	3.97×10^{-5}	9.12×10^{-3}	92.8

TABLE II: For each GST analysis of the qubit-pairs, we present the single qubit fidelity of an $R_X(\pi/2)$ gate on the first qubit; the two-qubit CNOT fidelity; and the theoretical error given by the POST tune-up scheme; the estimated infidelity; and the estimated improvement. The estimated improvement figures are calculated with r_c given by the product of the theoretical fidelity of the tuned-up CNOT with the actual fidelities of two single qubit gates on the control – this puts a loose upper bound on the improvement that can be expected. Highlighted in blue is the 14-9 qubit pair on which we experimentally tested the POST scheme, see Figure 3.

DISCUSSION

The transition from mathematical maps to physical operations is not always a seamless one. Besides errors in the GST characterisation, absent a good method of characterising non-Markovian behaviour, assumptions must be made of weak system-environment correlations, composability of operations, and minimal cross-talk between qubits. The emergence of unexpected behaviour from quantum systems means that in-principle operational improvements, such as the direct application of corrections from GST estimates, cannot always be relied upon. We have presented a general quantum-classical hybrid method which uses the real-life performance of the gate as the feed-forward for corrective updates. The success of the procedure is therefore self-fulfilling.

Randomised benchmarking is a robust method of measuring the Markovian fidelity of a given operation. However, in a system with environmental back-action or context dependent gates, it is not clear whether the situation will always be so simple as transplanting a redefined gate into a quantum circuit and seeing an increased fidelity in this new context. The markedly better performance of quantum algorithms consisting of these redefined gates remains to be demonstrated and will be the subject of future work. In particular, the POST algorithm would be easily adapted to any characterisation technique more inclusive of non-Markovian behaviour.

Developing high-fidelity gate hardware is imperative for the field of quantum computing to achieve its ambitious aims. An underrated measure of device quality, however, is *consistency* – the ability to achieve reported minimal error rates again and again despite gradual changes in device parameters and system-environment correlations. In this work we presented a consistent method that combines an initial overhead of gate set tomography with a classical optimisation algorithm that delivers an improved two-qubit gate in relatively few experiments. We emphasise that although POST was

tested on an *IBM Q* device, it is applicable to any hardware with logical-level control. Furthermore, the method is adaptable to any level of control. The key aspect is identifying noisy parameters from the GST estimate using the afforded set of device controls. In particular, we would expect to see significantly better results with pulse-level control wherein instead of separately implementing the corrective unitaries, they would be absorbed into modifying the CNOT pulse, there would be minimal additional gate errors introduced, or increase in depth.

ACKNOWLEDGMENTS

We are grateful to K. Modi and F. Pollock for valuable conversations, and to D. Broadway for figure advice. This work was supported by the University of Melbourne through the establishment of an IBM Network Q Hub at the University, and the Laby Foundation.

REFERENCES

-
- * loydch@unimelb.edu.au
- [1] Robin Blume-Kohout, John King Gamble, Erik Nielsen, Kenneth Rudinger, Jonathan Mizrahi, Kevin Fortier, and Peter Maunz. Demonstration of qubit operations below a rigorous fault tolerance threshold with gate set tomography. *Nature Communications*, 8:1–13, 2017.
 - [2] Frank Arute et al. Quantum supremacy using a programmable superconducting processor. *Nature*, 574(July), 2019.
 - [3] Chris Nay. IBM Opens Quantum Computation Center in New York; Brings World’s Largest Fleet of

- Quantum Computing Systems Online, Unveils New 53-Qubit Quantum System for Broad Use, 2019.
- [4] Jeremy Hsu. Intel’s 49-Qubit Chip Shoots for Quantum Supremacy, 2018.
- [5] Will Zeng. Unsupervised Machine Learning on Rigetti 19Q with Forest 1.2, 2017.
- [6] R Barends et al. Superconducting quantum circuits at the surface code threshold for fault tolerance. *Nature*, 508:500, 4 2014.
- [7] Jonas Zeuner, Aditya N. Sharma, Max Tillmann, Ren Heilmann, Markus Gräfe, Amir M-qanaki, Alexander Szameit, and Philip Walther. Integrated-optics heralded controlled-NOT gate for polarization-encoded qubits. *npj Quantum Information*, 4(1), 2018.
- [8] T P Harty, M A Sepiol, D T C Allcock, C J Ballance, J E Tarlton, and D M Lucas. High-Fidelity Trapped-Ion Quantum Logic Using Near-Field Microwaves. *Phys. Rev. Lett.*, 117(14):140501, 9 2016.
- [9] Y He, S K Gorman, D Keith, L Kranz, J G Keizer, and M Y Simmons. A two-qubit gate between phosphorus donor electrons in silicon. *Nature*, 571(7765):371–375, 2019.
- [10] Sabrina S. Hong et al. Demonstration of a Parametrically-Activated Entangling Gate Protected from Flux Noise. 2019.
- [11] Morten Kjaergaard, Mollie E. Schwartz, Jochen Braumüller, Philip Krantz, Joel I-Jan Wang, Simon Gustavsson, and William D. Oliver. Superconducting Qubits: Current State of Play. pages 1–28, 2019.
- [12] C. E. Bradley, J. Randall, M. H. Abobeih, R. C. Berrevoets, M. J. Degen, M. A. Bakker, M. Markham, D. J. Twitchen, and T. H. Taminiau. A Ten-Qubit Solid-State Spin Register with Quantum Memory up to One Minute. *Physical Review X*, 9(3):31045, 2019.
- [13] P. V. Klimov et al. Fluctuations of Energy-Relaxation Times in Superconducting Qubits. *Physical Review Letters*, 121(9):90502, 2018.
- [14] M. A. Fogarty, M. Veldhorst, R. Harper, C. H. Yang, S. D. Bartlett, S. T. Flammia, and A. S. Dzurak. Nonexponential fidelity decay in randomized benchmarking with low-frequency noise. *Physical Review A - Atomic, Molecular, and Optical Physics*, 92(2):1–7, 2015.
- [15] J. M. Chow, J. M. Gambetta, L. Tornberg, Jens Koch, Lev S. Bishop, A. A. Houck, B. R. Johnson, L. Frunzio, S. M. Girvin, and R. J. Schoelkopf. Randomized benchmarking and process tomography for gate errors in a solid-state qubit. *Physical Review Letters*, 102(9):1–4, 2009.
- [16] J F Poyatos, J I Cirac, and P Zoller. Complete Characterization of a Quantum Process: The Two-Bit Quantum Gate. *Phys. Rev. Lett.*, 78(2):390–393, 1 1997.
- [17] E. Knill, D. Leibfried, R. Reichle, J. Britton, R. B. Blakestad, J. D. Jost, C. Langer, R. Ozeri, S. Seidelin, and D. J. Wineland. Randomized benchmarking of quantum gates. *Physical Review A - Atomic, Molecular, and Optical Physics*, 77(1):12307, 1 2008.
- [18] Robin Blume-Kohout, John Gamble, Erik Nielsen, Jonathan Mizrahi, Jonathan Sterk, and Peter Maunz. Robust, self-consistent, closed-form tomography of quantum logic gates on a trapped ion qubit. 2013.
- [19] Seth T Merkel, Jay M Gambetta, John A Smolin, Stefano Poletto, Antonio D Córcoles, Blake R Johnson, Colm A Ryan, and Matthias Steffen. Self-consistent quantum process tomography. *Phys. Rev. A*, 87(6):62119, 6 2013.
- [20] Peter Lukas Wilhelm Maunz. Characterization of Two-Qubit Quantum Gates in Sandia’s High Optical Access surface ion trap. 2016.
- [21] Shuaining Zhang, Yao Lu, Kuan Zhang, Wentao Chen, Ying Li, Jing-ning Zhang, and Kihwan Kim. Error-Mitigated Quantum Gates Exceeding Physical Fidelities in a Trapped-Ion System. pages 1–10, 2019.
- [22] Chao Song, Jing Cui, H. Wang, J. Hao, H. Feng, and Ying Li. Quantum computation with universal error mitigation on a superconducting quantum processor. *Science Advances*, 5(9):eaaw5686, 2019.
- [23] Suguru Endo, Simon C. Benjamin, and Ying Li. Practical Quantum Error Mitigation for Near-Future Applications. *Physical Review X*, 8(3):31027, 2018.
- [24] T E OBrien, B Tarasinski, and L DiCarlo. Density-matrix simulation of small surface codes under current and projected experimental noise. *npj Quantum Information*, 3(1):39, 2017.
- [25] Daniel Greenbaum. Introduction to Quantum Gate Set Tomography. 2015.
- [26] Thomas F Jordan. Maps and inverse maps in open quantum dynamics. *Annals of Physics*, 325(10):2075–2089, 2010.
- [27] Kristan Temme, Sergey Bravyi, and Jay M. Gambetta. Error Mitigation for Short-Depth Quantum Circuits. *Physical Review Letters*, 119(18):1–5, 2017.
- [28] Erik Nielsen, Robin J Blume-Kohout, Kenneth M Rudinger, Timothy J Proctor, Lucas Saldyt, and USDOE. Python GST Implementation (PyGSTi) v. 0.9, Version v. 0.9, 2019.
- [29] Fuchang Gao and Lixing Han. Implementing the Nelder-Mead simplex algorithm with adaptive parameters. *Computational Optimization and Applications*, 51(1):259–277, 2012.
- [30] Timothy J Proctor, Arnaud Carignan-Dugas, Kenneth Rudinger, Erik Nielsen, Robin Blume-Kohout, and Kevin Young. Direct Randomized Benchmarking for Multiqubit Devices. *Phys. Rev. Lett.*, 123(3):30503, 7 2019.